Search for $\Omega(2012) \to K\Xi(1530) \to K\pi\Xi$ at Belle

S. Jia,[2] C. P. Shen,[11] I. Adachi,[19,15] J. K. Ahn,[41] H. Aihara,[88] S. Al Said,[83,38] D. M. Asner,[3] T. Aushev,[57] R. Ayad,[83] V. Babu,[8] S. Bahinipati,[24] A. M. Bakich,[82] P. Behera,[27] C. Beleño,[14] J. Bennett,[54] M. Berger,[80] V. Bhardwaj,[23] T. Bilka,[5] J. Biswal,[35] A. Bobrov,[4,68] A. Bozek,[65] M. Bračko,[51,35] T. E. Browder,[18] M. Campajola,[32,60] L. Cao,[36] D. Červenkov,[5] V. Chekelian,[52] A. Chen,[62] B. G. Cheon,[17] K. Chilikin,[46] H. E. Cho,[17] K. Cho,[40] S.-K. Choi,[16] Y. Choi,[81] S. Choudhury,[26] D. Cinabro,[92] S. Cunliffe,[8] N. Dash,[24] G. De Nardo,[32,60] F. Di Capua,[32,60] S. Di Carlo,[44] Z. Doležal,[5] T. V. Dong,[19,15] S. Eidelman,[4,68,46] D. Epifanov,[4,68] J. E. Fast,[70] B. G. Fulsom,[70] V. Gaur,[91] N. Gabyshev,[4,68] A. Garmash,[4,68] A. Giri,[26] P. Goldenzweig,[36] B. Golob,[47,35] O. Grzymkowska,[65] O. Hartbrich,[18] K. Hayasaka,[67] H. Hayashii,[61] W.-S. Hou,[64] K. Huang,[64] T. Iijima,[59,58] K. Inami,[58] G. Inguglia,[30] A. Ishikawa,[19] R. Itoh,[19,15] M. Iwasaki,[69] Y. Iwasaki,[19] W. W. Jacobs,[28] Y. Jin,[88] D. Joffe,[37] K. K. Joo,[6] A. B. Kaliyar,[27] K. H. Kang,[43] G. Karyan,[8] Y. Kato,[58] T. Kawasaki,[39] H. Kichimi,[19] D. Y. Kim,[79] H. J. Kim,[43] K. T. Kim,[41] S. H. Kim,[17] K. Kinoshita,[7] P. Kodyš,[5] S. Korpar,[51,35] D. Kotchetkov,[18] P. Križan,[47,35] R. Kroeger,[54] P. Krokovny,[4,68] R. Kumar,[73] A. Kuzmin,[4,68] Y.-J. Kwon,[94] J. S. Lange,[12] I. S. Lee,[17] J. K. Lee,[77] J. Y. Lee,[77] S. C. Lee,[43] L. K. Li,[29] Y. B. Li,[71] L. Li Gioi,[52] J. Libby,[27] K. Lieret,[48] D. Liventsev,[91,19] P.-C. Lu,[64] J. MacNaughton,[55] C. MacQueen,[53] M. Masuda,[87] T. Matsuda,[55] D. Matvienko,[4,68,46] J. T. McNeil,[10] M. Merola,[32,60] H. Miyata,[67] R. Mizuk,[46,57] T. Mori,[58] R. Mussa,[33] T. Nakano,[74] M. Nakao,[19,15] K. J. Nath,[25] M. Nayak,[92,19] M. Niiyama,[42] N. K. Nisar,[72] S. Nishida,[19,15] K. Nishimura,[18] K. Ogawa,[67] S. Ogawa,[85] H. Ono,[66,67] Y. Onuki,[88] W. Ostrowicz,[65] P. Pakhlov,[46,56] G. Pakhlova,[46,57] B. Pal,[3] T. Pang,[72] S. Pardi,[32] S.-H. Park,[94] S. Patra,[23] S. Paul,[84] T. K. Pedlar,[49] R. Pestotnik,[35] L. E. Piilonen,[91] V. Popov,[46,57] E. Prencipe,[21] M. Ritter,[48] A. Rostomyan,[8] G. Russo,[60] Y. Sakai,[19,15] M. Salehi,[50,48] S. Sandilya,[7] L. Santelj,[19] T. Sanuki,[86] V. Savinov,[72] O. Schneider,[45] G. Schnell,[1,22] J. Schueler,[18] C. Schwanda,[30] Y. Seino,[67] K. Senyo,[93] O. Seon,[58] M. E. Sevior,[53] V. Shebalin,[18] J.-G. Shiu,[64] A. Sokolov,[31] E. Solovieva,[46] M. Starič,[35] J. F. Strube,[70] M. Sumihama,[13] T. Sumiyoshi,[90] W. Sutcliffe,[36] M. Takizawa,[78,20,75] U. Tamponi,[33] K. Tanida,[34] F. Tenchini,[8] M. Uchida,[89] T. Uglov,[46,57] Y. Unno,[17] S. Uno,[19,15] P. Urquijo,[53] Y. Usov,[4,68] S. E. Vahsen,[18] R. Van Tonder,[36] G. Varner,[18] A. Vinokurova,[4,68] A. Vossen,[9] B. Wang,[52] C. H. Wang,[63] M.-Z. Wang,[64] P. Wang,[29] E. Won,[41] S. B. Yang,[41] H. Ye,[8] J. Yelton,[10] J. H. Yin,[29] C. Z. Yuan,[29] Y. Yusa,[67] Z. P. Zhang,[76] V. Zhilich,[4,68] and V. Zhukova[46]

(Belle Collaboration)

[1]*University of the Basque Country UPV/EHU, 48080 Bilbao*
[2]*Beihang University, Beijing 100191*
[3]*Brookhaven National Laboratory, Upton, New York 11973*
[4]*Budker Institute of Nuclear Physics SB RAS, Novosibirsk 630090*
[5]*Faculty of Mathematics and Physics, Charles University, 121 16 Prague*
[6]*Chonnam National University, Kwangju 660-701*
[7]*University of Cincinnati, Cincinnati, Ohio 45221*
[8]*Deutsches Elektronen–Synchrotron, 22607 Hamburg*
[9]*Duke University, Durham, North Carolina 27708*
[10]*University of Florida, Gainesville, Florida 32611*
[11]*Key Laboratory of Nuclear Physics and Ion-beam Application (MOE) and Institute of Modern Physics, Fudan University, Shanghai 200443*
[12]*Justus-Liebig-Universität Gießen, 35392 Gießen*
[13]*Gifu University, Gifu 501-1193*
[14]*II. Physikalisches Institut, Georg-August-Universität Göttingen, 37073 Göttingen*
[15]*SOKENDAI (The Graduate University for Advanced Studies), Hayama 240-0193*
[16]*Gyeongsang National University, Chinju 660-701*
[17]*Hanyang University, Seoul 133-791*
[18]*University of Hawaii, Honolulu, Hawaii 96822*
[19]*High Energy Accelerator Research Organization (KEK), Tsukuba 305-0801*
[20]*J-PARC Branch, KEK Theory Center, High Energy Accelerator Research Organization (KEK), Tsukuba 305-0801*
[21]*Forschungszentrum Jülich, 52425 Jülich*
[22]*IKERBASQUE, Basque Foundation for Science, 48013 Bilbao*
[23]*Indian Institute of Science Education and Research Mohali, SAS Nagar, 140306*
[24]*Indian Institute of Technology Bhubaneswar, Satya Nagar 751007*
[25]*Indian Institute of Technology Guwahati, Assam 781039*

[26]*Indian Institute of Technology Hyderabad, Telangana 502285*
[27]*Indian Institute of Technology Madras, Chennai 600036*
[28]*Indiana University, Bloomington, Indiana 47408*
[29]*Institute of High Energy Physics, Chinese Academy of Sciences, Beijing 100049*
[30]*Institute of High Energy Physics, Vienna 1050*
[31]*Institute for High Energy Physics, Protvino 142281*
[32]*INFN—Sezione di Napoli, 80126 Napoli*
[33]*INFN—Sezione di Torino, 10125 Torino*
[34]*Advanced Science Research Center, Japan Atomic Energy Agency, Naka 319-1195*
[35]*J. Stefan Institute, 1000 Ljubljana*
[36]*Institut für Experimentelle Teilchenphysik, Karlsruher Institut für Technologie, 76131 Karlsruhe*
[37]*Kennesaw State University, Kennesaw, Georgia 30144*
[38]*Department of Physics, Faculty of Science, King Abdulaziz University, Jeddah 21589*
[39]*Kitasato University, Sagamihara 252-0373*
[40]*Korea Institute of Science and Technology Information, Daejeon 305-806*
[41]*Korea University, Seoul 136-713*
[42]*Kyoto University, Kyoto 606-8502*
[43]*Kyungpook National University, Daegu 702-701*
[44]*LAL, Univ. Paris-Sud, CNRS/IN2P3, Université Paris-Saclay, Orsay*
[45]*École Polytechnique Fédérale de Lausanne (EPFL), Lausanne 1015*
[46]*P.N. Lebedev Physical Institute of the Russian Academy of Sciences, Moscow 119991*
[47]*Faculty of Mathematics and Physics, University of Ljubljana, 1000 Ljubljana*
[48]*Ludwig Maximilians University, 80539 Munich*
[49]*Luther College, Decorah, Iowa 52101*
[50]*University of Malaya, 50603 Kuala Lumpur*
[51]*University of Maribor, 2000 Maribor*
[52]*Max-Planck-Institut für Physik, 80805 München*
[53]*School of Physics, University of Melbourne, Victoria 3010*
[54]*University of Mississippi, University, Mississippi 38677*
[55]*University of Miyazaki, Miyazaki 889-2192*
[56]*Moscow Physical Engineering Institute, Moscow 115409*
[57]*Moscow Institute of Physics and Technology, Moscow Region 141700*
[58]*Graduate School of Science, Nagoya University, Nagoya 464-8602*
[59]*Kobayashi-Maskawa Institute, Nagoya University, Nagoya 464-8602*
[60]*Università di Napoli Federico II, 80055 Napoli*
[61]*Nara Women's University, Nara 630-8506*
[62]*National Central University, Chung-li 32054*
[63]*National United University, Miao Li 36003*
[64]*Department of Physics, National Taiwan University, Taipei 10617*
[65]*H. Niewodniczanski Institute of Nuclear Physics, Krakow 31-342*
[66]*Nippon Dental University, Niigata 951-8580*
[67]*Niigata University, Niigata 950-2181*
[68]*Novosibirsk State University, Novosibirsk 630090*
[69]*Osaka City University, Osaka 558-8585*
[70]*Pacific Northwest National Laboratory, Richland, Washington 99352*
[71]*Peking University, Beijing 100871*
[72]*University of Pittsburgh, Pittsburgh, Pennsylvania 15260*
[73]*Punjab Agricultural University, Ludhiana 141004*
[74]*Research Center for Nuclear Physics, Osaka University, Osaka 567-0047*
[75]*Theoretical Research Division, Nishina Center, RIKEN, Saitama 351-0198*
[76]*University of Science and Technology of China, Hefei 230026*
[77]*Seoul National University, Seoul 151-742*
[78]*Showa Pharmaceutical University, Tokyo 194-8543*
[79]*Soongsil University, Seoul 156-743*
[80]*Stefan Meyer Institute for Subatomic Physics, Vienna 1090*
[81]*Sungkyunkwan University, Suwon 440-746*
[82]*School of Physics, University of Sydney, New South Wales 2006*
[83]*Department of Physics, Faculty of Science, University of Tabuk, Tabuk 71451*
[84]*Department of Physics, Technische Universität München, 85748 Garching*
[85]*Toho University, Funabashi 274-8510*

[86]*Department of Physics, Tohoku University, Sendai 980-8578*
[87]*Earthquake Research Institute, University of Tokyo, Tokyo 113-0032*
[88]*Department of Physics, University of Tokyo, Tokyo 113-0033*
[89]*Tokyo Institute of Technology, Tokyo 152-8550*
[90]*Tokyo Metropolitan University, Tokyo 192-0397*
[91]*Virginia Polytechnic Institute and State University, Blacksburg, Virginia 24061*
[92]*Wayne State University, Detroit, Michigan 48202*
[93]*Yamagata University, Yamagata 990-8560*
[94]*Yonsei University, Seoul 120-749*

(Received 1 June 2019; published 19 August 2019)

Using data samples of e^+e^- collisions collected at the $\Upsilon(1S)$, $\Upsilon(2S)$, and $\Upsilon(3S)$ resonances with the Belle detector, we search for the three-body decay of the $\Omega(2012)$ baryon to $K\pi\Xi$. This decay is predicted to dominate for models describing the $\Omega(2012)$ as a $K\Xi(1530)$ molecule. No significant $\Omega(2012)$ signals are observed in the studied channels, and 90% credibility level upper limits on the ratios of the branching fractions relative to $K\Xi$ decay modes are obtained.

DOI: 10.1103/PhysRevD.100.032006

I. INTRODUCTION

Very recently a new state, the excited $\Omega(2012)$ baryon, has been observed by the Belle collaboration [1] in the ΞK invariant mass spectra using data samples collected at the $\Upsilon(1S, 2S, 3S)$ energies, with measured mass $M = [2012.4 \pm 0.7(\text{stat}) \pm 0.6(\text{syst})]\ \text{MeV}/c^2$ and width $\Gamma = [6.4 \pm 2.5(\text{stat}) \pm 1.6(\text{syst})]\ \text{MeV}$. The observed spacing in the Ω mass spectrum between the ground state and this excited state ($\sim$340 MeV/c^2) is smaller than that for other Ω^- excited states [2], and is more similar to the negative-parity orbital excitations of many other baryon pairs such as Λ and $\Lambda(1405)$ or Λ_c^+ and $\Lambda_c^+(2595)$.

After the initial observation of the $\Omega(2012)$, several theoretical interpretations of that state were offered [3–11]. Although it is generally accepted that $\Omega(2012)$ is a $1P$ orbital excitation of the ground-state Ω baryon with quark content sss and quantum numbers $J^P = \frac{3}{2}^-$, Refs. [7–10] propose an alternative interpretation as a $K\Xi(1530)$ hadronic molecule. These models predict a large decay width for $\Omega(2012) \to K\pi\Xi$. In Ref. [7], the decay $\Omega(2012) \to K\pi\Xi$ is predicted to dominate over $\Omega(2012) \to K\Xi$, while in Refs. [8–10], the production rates of the $\Omega(2012)$ are almost similar in $K\pi\Xi$ and $K\Xi$ decay channels. The authors in Ref. [11] also discuss the three-body decay of the $\Omega(2012)$. They regard $\Omega(2012)$ as a member of the compact decuplet states only if the sum of branching fractions of the $\Omega(2012) \to K\pi\Xi$ and $\Omega(2012) \to \Omega\pi\pi$ is not too large ($< 70\%$).

In this paper, we report on a search for $\Omega(2012) \to K\Xi(1530) \to K\pi\Xi$ using $\Upsilon(1S, 2S, 3S)$ data samples collected by the Belle experiment at the KEKB asymmetric-energy e^+e^- collider [12,13]. Note that charge-conjugate modes are implied throughout, unless explicitly stated otherwise.

II. THE DATA SAMPLE AND BELLE DETECTOR

The Belle data used in this analysis correspond to 5.7 fb^{-1} of integrated luminosity at the $\Upsilon(1S)$ resonance, 24.9 fb^{-1} at the $\Upsilon(2S)$ resonance, and 2.9 fb^{-1} at the $\Upsilon(3S)$ resonance. The Belle detector [14,15] is a large solid-angle magnetic spectrometer consisting of a silicon vertex detector (SVD), a 50-layer central drift chamber (CDC), an array of aerogel threshold Cherenkov counters (ACC), a barrellike arrangement of time-of-flight scintillation counters (TOF), and an electromagnetic calorimeter comprised of CsI(Tl) crystals (ECL) located inside a superconducting solenoid coil providing a 1.5 T magnetic field. An iron flux-return yoke instrumented with resistive plate chambers (KLM) located outside the coil is used to detect K_L^0 mesons and to identify muons.

Large signal Monte Carlo (MC) samples (1 million events for each studied process) are generated using the EVTGEN [16] code to simulate the expected signal event topology and estimate the signal detection efficiency. The processes $\Upsilon(1S, 2S, 3S) \to \Omega(2012) + anything \to K\Xi(1530) + anything \to K\pi\Xi + anything$ are simulated; the mass and width of $\Omega(2012)$ are fixed at 2.0124 GeV/c^2 and 6.4 MeV [1], respectively. To assess possible backgrounds arising from the continuum ($e^+e^- \to q\bar{q}$ with $q = u, d, s, c$), we generate such events at center-of-mass energies of $\Upsilon(1S)$, $\Upsilon(2S)$, and $\Upsilon(3S)$ resonances using the Lund fragmentation model in PYTHIA [17]. Inclusive $\Upsilon(1S)$ and $\Upsilon(2S)$ MC samples, corresponding to four times the

luminosity of the data, are produced using PYTHIA and are used to identify possible peaking backgrounds from $\Upsilon(1S)$ and $\Upsilon(2S)$ decays.

III. SEARCH FOR $\Omega(2012) \to K\Xi(1530) \to K\pi\Xi$

A. Event selection

The combined information from the CDC, TOF, and ACC is used to identify charged kaons and pions based on the kaon likelihood ratio, $R_K = \mathcal{L}_K/(\mathcal{L}_K + \mathcal{L}_\pi)$, where $\mathcal{L}_K$ and $\mathcal{L}_\pi$ are the likelihood values for the kaon and pion hypotheses, respectively. Tracks with $R_K = \mathcal{L}_K/(\mathcal{L}_K + \mathcal{L}_\pi) < 0.4$ are identified as pions with an efficiency of 96%, while 8% of kaons are misidentified as pions; tracks with $R_K > 0.6$ are identified as kaons with an efficiency of 95%, while 6% of pions are misidentified as kaons.

An ECL cluster is treated as a photon candidate if it does not match the extrapolation of any charged track reconstructed by the tracking systems (CDC and SVD) into the calorimeter. The π^0 candidates are reconstructed from two photons having energy exceeding 50 MeV in the barrel or 100 MeV in the endcaps. To avoid contamination from neutral hadrons, we reject neutral showers if the ratio of the energy deposited in the central array of 3×3 ECL cells to that deposited in the surrounding array of 5×5 cells is less than 0.8. The $\pi^0 \to \gamma\gamma$ candidates are also required to have an energy balance parameter $|E_1 - E_2|/(E_1 + E_2)$ smaller than 0.8, where E_1 (E_2) is the energy of the first (second) photon in the laboratory frame. To further reduce the combinatorial background, the momentum of the π^0 candidate is required to exceed 200 MeV/c. We define the π^0 signal region as $|M_{\gamma\gamma} - m_{\pi^0}| < 12$ MeV/c^2 ($\sim 2\sigma$), where m_{π^0} is the π^0 nominal mass [2]. For each selected π^0 candidate a mass-constrained fit is performed to improve its momentum resolution.

The K_S^0 candidates are reconstructed via the $K_S^0 \to \pi^+\pi^-$ decay, and the identification is enhanced by selecting on the outputs of a neural network [18]. The network uses the following input variables [19]: the K_S^0 momentum in the lab frame, the distance along the z axis between the two track helices at their closest approach, the K_S^0 flight length in the $r - \phi$ plane, the angle between the K_S^0 momentum and the vector joining the interaction point (IP) to the K_S^0 decay vertex, the angle between the pion momentum and the lab frame direction in the K_S^0 rest frame, the distances of closest approach in the $r - \phi$ plane between the IP and the two pion helices, the number of hits in the CDC for each pion track, and the presence or absence of hits in the SVD for each pion track.

Candidate Λ decays are reconstructed from $p\pi^-$ pairs with a production vertex significantly separated from the IP. For the $\Xi^-(\to \Lambda\pi^-)$ and $\Xi^0(\to \Lambda\pi^0)$ candidates, the vertex fits are performed and the positive Ξ^- and Ξ^0 flight distances are required. The selected $\Xi^-(\to \Lambda\pi^-)$ and $\Xi^0(\to \Lambda\pi^0)$ candidates are the same as those in Ref. [1]. The Ξ^-

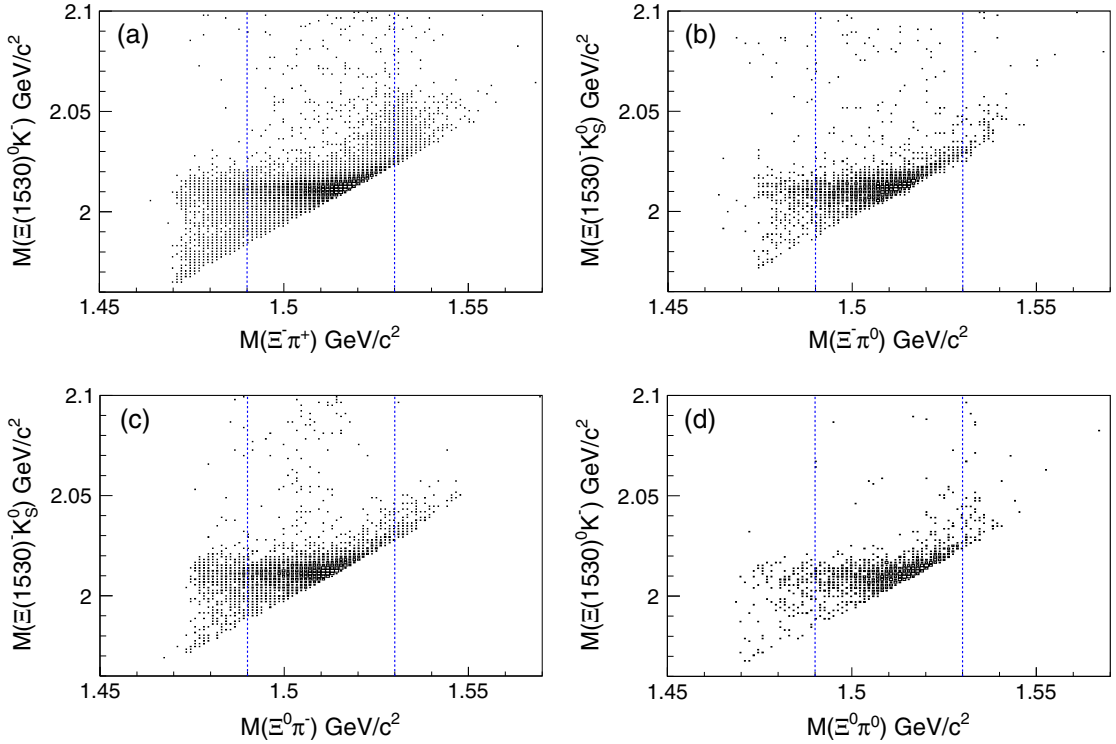

FIG. 1. Distributions of (a) $M(\Xi(1530)^0K^-)$ versus $M(\Xi^-\pi^+)$, (a) $M(\Xi(1530)^-K_S^0)$ versus $M(\Xi^-\pi^0)$, (a) $M(\Xi(1530)^-K_S^0)$ versus $M(\Xi^0\pi^-)$, and (d) $M(\Xi(1530)^0K^-)$ versus $M(\Xi^0\pi^0)$ from signal MC samples. The dotted lines bound the $\Xi(1530)$ signal region.

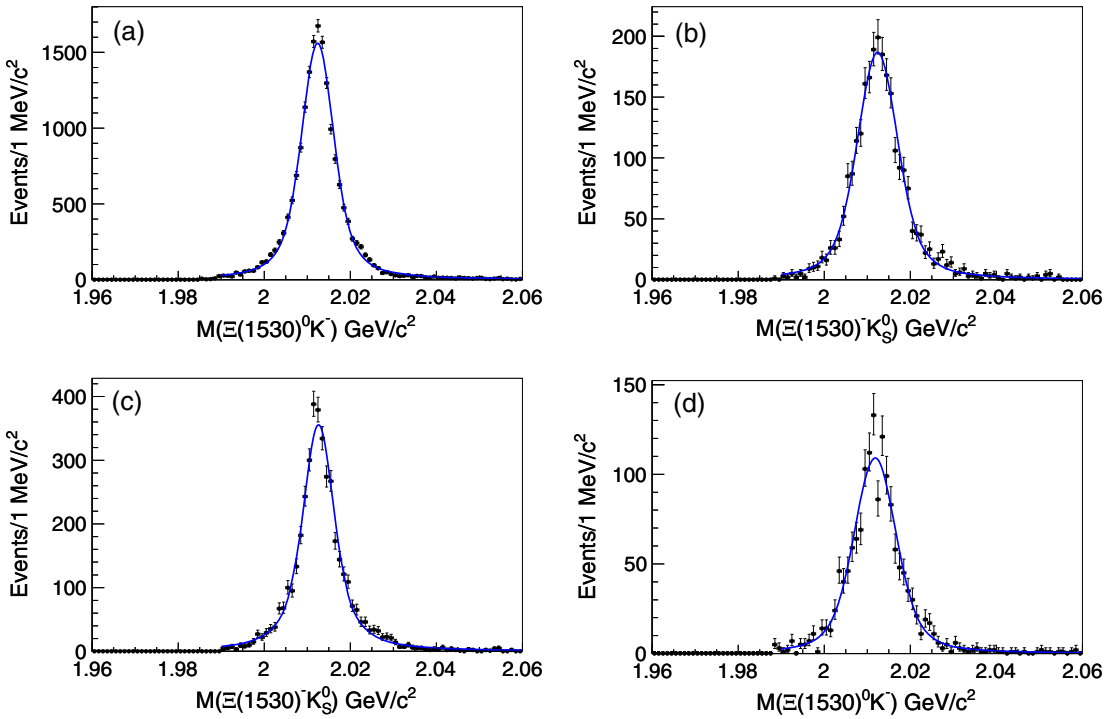

FIG. 2. The distributions of the invariant mass of (a) $\Xi(1530)^0(\to \Xi^-\pi^+)K^-$, (b) $\Xi(1530)^-(\to \Xi^-\pi^0)K^0_S$, (c) $\Xi(1530)^-(\to \Xi^0\pi^-)K^0_S$, and (d) $\Xi(1530)^0(\to \Xi^0\pi^0)K^-$ in the signal MC samples. The solid curves show the fitted results.

and Ξ^0 are kinematically constrained to their nominal masses [2], and then combined with a $\pi^\pm$ or π^0 to form a $\Xi(1530)^-$ or $\Xi(1530)^0$ candidate. Finally, the selected $\Xi(1530)$ candidate is combined with a K^- or K^0_S to form the $\Omega(2012)$ candidate. In this last step, a vertex fit is performed for the $K\pi\Xi$ final state to improve the momentum resolutions and suppress the backgrounds, requiring $\chi^2_{\rm vertex} < 20$, corresponding to an estimated selection efficiency exceeding 95%. Reconstruction spans the $\Omega(2012)^- \to \Xi^-\pi^+K^-$, $\Xi^-\pi^0K^0_S$, $\Xi^0\pi^-K^0_S$, and $\Xi^0\pi^0K^-$ three-body decay modes of $\Omega(2012)$.

Before searching for $\Omega(2012) \to K\Xi(1530) \to K\pi\Xi$, a cross-check on the previously reconstructed $\Omega(2012) \to \Xi K$ decay mode is performed. Selection of $\Omega(2012)^- \to \Xi^-K^0_S/\Xi^0K^-$ candidates uses well-reconstructed tracks, particle identifications, and vertex fitting technique in a way similar to the methods in Ref. [1]. As a result, the signal yields from the simultaneous fit of the $\Omega(2012)^- \to \Xi^-K^0_S$ and $\Omega(2012)^- \to \Xi^0K^-$ are 283 ± 72 and 239 ± 47, respectively. The obtained mass and width for the $\Omega(2012)$ are $M = (2012.1 \pm 0.7)$ MeV/c^2 and $\Gamma = (6.9^{+2.5}_{-2.0})$ MeV, where the uncertainties are statistical only. Our results are consistent with those in Ref. [1] within errors.

B. The distributions from signal MC samples

After all event selection requirements, Fig. 1 shows the distributions of the $\Xi\pi K$ invariant mass versus the $\Xi\pi$ invariant mass from signal MC samples. Due to phase space limitations, events at high $\Xi\pi$ and/or low $\Xi\pi K$ mass are kinematically forbidden. We define the optimized $\Xi(1530)$ signal region as 1.49 GeV/$c^2 < M(\Xi\pi) <$ 1.53 GeV/c^2 (discussed below), between the blue dashed lines in Fig. 1.

The invariant mass distributions from MC signal simulations of $\Xi(1530)^0(\to \Xi^-\pi^+/\Xi^0\pi^0)K^-$ and $\Xi(1530)^-(\to \Xi^-\pi^0/\Xi^0\pi^-)K^0_S$ are shown in Fig. 2. The signal shape of the $\Omega(2012)$ is described by a Breit-Wigner (BW) function convolved with a Gaussian function, where the BW mass and width are fixed to 2.0124 GeV/c^2 and 6.4 MeV [1], respectively, and the mass-resolution, i.e., Gaussian width is determined in the fit.

C. $\Xi(1530)$ signals in $\Upsilon(1S,2S,3S)$ data

After imposing our selection criteria, the invariant mass spectra of $\Xi(1530)^0 \to \Xi^-\pi^+, \Xi^0\pi^0$, and $\Xi(1530)^- \to \Xi^-\pi^0$, $\Xi^0\pi^-$ candidates are shown in Figs. 3(a)–3(d). Clear signals of $\Xi(1530)^0$ and $\Xi(1530)^-$ are observed in the modes $\Xi(1530)^0 \to \Xi^-\pi^+$ and $\Xi(1530)^- \to \Xi^-\pi^0$, $\Xi^0\pi^-$.

We fit all the invariant mass distributions, modeling the $\Xi(1530)$ peaks with the convolution of a BW and a Gaussian function and the background as a second-order polynomial. In the fits, the BW parameters are unconstrained, while the Gaussian widths are fixed according to MC simulations. The fit values are consistent with the world averages within their respective errors [2]. For $\Xi(1530)^0 \to \Xi^0\pi^0$, the mass and width of $\Xi(1530)^0$ are

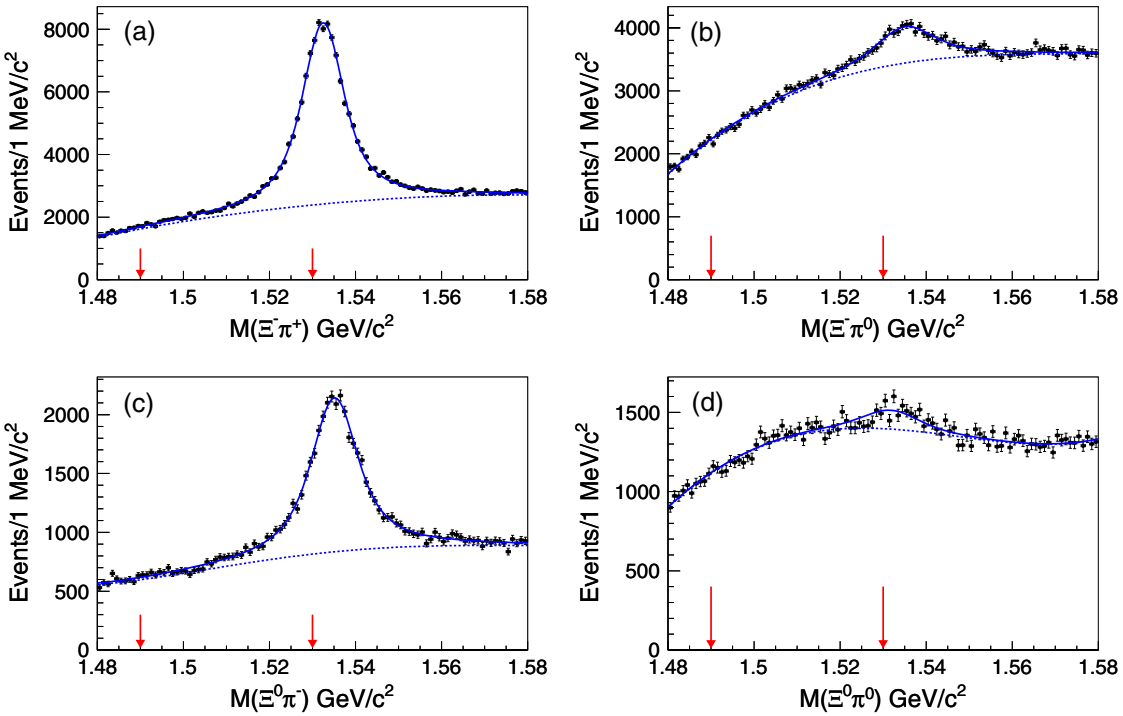

FIG. 3. Invariant mass distributions for (a) $\Xi(1530)^0 \to \Xi^-\pi^+$, (b) $\Xi(1530)^- \to \Xi^-\pi^0$, (c) $\Xi(1530)^- \to \Xi^0\pi^-$, and (d) $\Xi(1530)^0 \to \Xi^0\pi^0$ candidates from the $\Upsilon(1S, 2S, 3S)$ data samples. Solid curves are the best fits, and dashed lines represent backgrounds. Red arrows indicate the $\Xi(1530)$ signal region for the $\Omega(2012)$ search, which is offset from the peak owing to the very limited allowed phase space.

fixed to the Particle Data Group (PDG) values [2] since the signal is not clear due to large combinatorial backgrounds. The results of the fits are listed in Table I.

D. $\Omega(2012) \to \Xi\pi K$ mass distributions in $\Upsilon(1S,2S,3S)$ data

Considering phase space limitations and our finite mass resolution, we require $1.49\ \mathrm{GeV}/c^2 < M(\Xi\pi) < 1.53\ \mathrm{GeV}/c^2$ to select $\Xi(1530)$ signals as efficiently as possible, as indicated by the red arrows in Fig. 3. We optimize this requirement by maximizing the figure of merit $N_{\mathrm{sig}}/\sqrt{N_{\mathrm{sig}}+N_{\mathrm{bkg}}}$ value with the mode $\Omega(2012)^- \to \Xi(1530)^0(\to \Xi^-\pi^+)K^-$, where N_{sig} is number of fitted signal events in the signal MC sample assuming $\mathcal{B}(\Upsilon(1S, 2S, 3S) \to \Omega(2012)^- + \mathrm{anything}) \times \mathcal{B}(\Omega(2012)^- \to \Xi(1530)^0 K^-) = 10^{-6}$ and N_{bkg} is the number of estimated background events in the $\Omega(2012)^-$ signal region using inclusive MC samples. The candidate signal region for the $\Xi(1530)$ coincides with the predicted mass interval from Ref. [9].

After application of the above selection criteria, Fig. 4 shows the invariant mass distributions of $\Xi(1530)^0(\to \Xi^-\pi^+/\Xi^0\pi^0)K^-$ and $\Xi(1530)^-(\to \Xi^-\pi^0/\Xi^0\pi^-)K^0_S$. From these distributions, no obvious $\Omega(2012)^-$ signal is observed. The shapes of the $\Omega(2012)$ signals in the fits are described by BW functions convolved with Gaussian resolution functions; the background shapes are described by a threshold function. The parameters of the BW functions are fixed to the mass and width of the $\Omega(2012)$ [1], and the mass resolutions are fixed to those from fits to signal MC samples (1.5, 2.6, 1.7, and 2.8 MeV for the $\Omega(2012) \to \Xi(1530)^0(\to \Xi^-\pi^+)K^-$, $\Xi(1530)^-(\to \Xi^-\pi^0)K^0_S$, $\Xi(1530)^-(\to \Xi^0\pi^-)K^0_S$, and $\Xi(1530)^0(\to \Xi^0\pi^0)K^-$ decay modes, respectively). The threshold function has the form $(M(\Xi K\pi)-x)^\alpha \exp[c_1(M(\Xi K\pi)-x)+c_2(M(\Xi K\pi)-x)^2]$,

TABLE I. Mass resolution from MC simulations, and the mass and width for inclusive $\Xi(1530)$ signals from fits to the Belle data.

Mode	Resolution (MeV/c^2)	Mass (MeV/c^2)	Width (MeV)
$\Xi(1530)^0 \to \Xi^-\pi^+$	2.34 ± 0.14	1532.47 ± 0.03	9.0 ± 0.3
$\Xi(1530)^- \to \Xi^-\pi^0$	2.96 ± 0.17	1535.07 ± 0.37	12.9 ± 1.8
$\Xi(1530)^- \to \Xi^0\pi^-$	2.44 ± 0.15	1535.11 ± 0.09	10.6 ± 0.2
$\Xi(1530)^0 \to \Xi^0\pi^0$	4.14 ± 0.26	1531.80 (PDG value)	9.1 (PDG value)

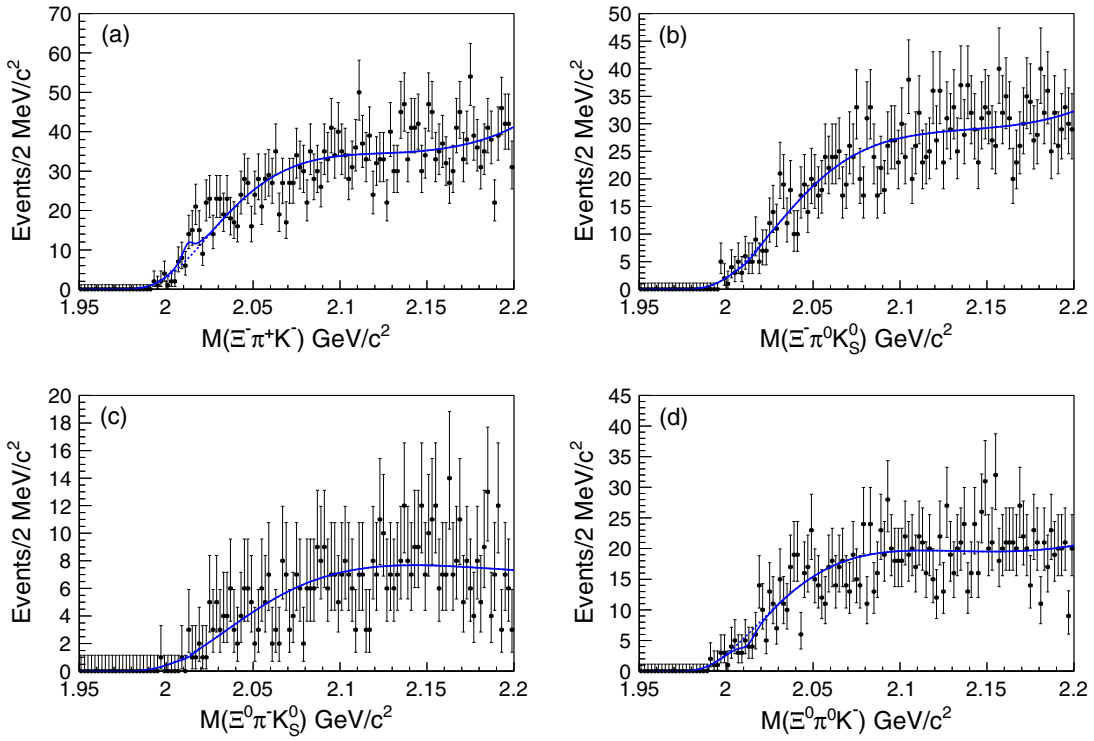

FIG. 4. The distributions of the invariant mass for (a) $\Xi(1530)^0(\to \Xi^-\pi^+)K^-$, (b) $\Xi(1530)^-(\to \Xi^-\pi^0)K^0_S$, (c) $\Xi(1530)^-(\to \Xi^0\pi^-)K^0_S$, and (d) $\Xi(1530)^0(\to \Xi^0\pi^0)K^-$ from the $\Upsilon(1S, 2S, 3S)$ data samples. The solid curves are the best fits, and the dashed lines represent the backgrounds.

where the parameters α, c_1, and c_2 are free; the threshold parameter x is fixed at 1.97 GeV/c^2 from the MC simulations. The yields of $\Omega(2012)$ signal events from the unbinned extended maximum-likelihood fits are obtained; they are listed in Table II, together with the reconstruction efficiency, signal significance, and the upper limit at 90% credibility level [20] (C.L.) on the signal yield for each $\Omega(2012)$ decay mode. In addition, no peaking backgrounds are found from the inclusive MC samples.

E. The ratios of the branching fractions for $\Omega(2012) \to K\pi\Xi$ relative to $K\Xi$

We define the ratios $\mathcal{R}^{\Xi^-\pi^+K^-}_{\Xi^-\bar{K}^0}$, $\mathcal{R}^{\Xi^-\pi^0\bar{K}^0}_{\Xi^-\bar{K}^0}$, $\mathcal{R}^{\Xi^0\pi^-\bar{K}^0}_{\Xi^0K^-}$, $\mathcal{R}^{\Xi^-\pi^+K^-}_{\Xi^0K^-}$, $\mathcal{R}^{\Xi^0\pi^-\bar{K}^0}_{\Xi^-\bar{K}^0}$, and $\mathcal{R}^{\Xi^0\pi^0K^-}_{\Xi^0K^-}$ and determine their values as follows:

$$\mathcal{R}^{\Xi^-\pi^+K^-}_{\Xi^-\bar{K}^0} = \frac{\mathcal{B}(\Omega(2012) \to \Xi(1530)^0(\to \Xi^-\pi^+)K^-)}{\mathcal{B}(\Omega(2012) \to \Xi^-\bar{K}^0)} = \frac{N_1^{\rm fit} \times \varepsilon_5 \times \mathcal{B}(K^0_S \to \pi^+\pi^-) \times \mathcal{B}(\bar{K}^0 \to K^0_S)}{N_5^{\rm fit} \times \varepsilon_1}, \quad (1)$$

$$\mathcal{R}^{\Xi^-\pi^0\bar{K}^0}_{\Xi^-\bar{K}^0} = \frac{\mathcal{B}(\Omega(2012) \to \Xi(1530)^-(\to \Xi^-\pi^0)\bar{K}^0)}{\mathcal{B}(\Omega(2012) \to \Xi^-\bar{K}^0)} = \frac{N_2^{\rm fit} \times \varepsilon_5}{N_5^{\rm fit} \times \varepsilon_2 \times \mathcal{B}(\pi^0 \to \gamma\gamma)}, \quad (2)$$

$$\mathcal{R}^{\Xi^0\pi^-\bar{K}^0}_{\Xi^0K^-} = \frac{\mathcal{B}(\Omega(2012) \to \Xi(1530)^-(\to \Xi^0\pi^-)\bar{K}^0)}{\mathcal{B}(\Omega(2012) \to \Xi^0K^-)} = \frac{N_3^{\rm fit} \times \varepsilon_6}{N_6^{\rm fit} \times \varepsilon_3 \times \mathcal{B}(K^0_S \to \pi^+\pi^-) \times \mathcal{B}(\bar{K}^0 \to K^0_S)}, \quad (3)$$

TABLE II. The reconstruction efficiency (ε), signal significance (σ), signal yield ($N^{\rm fit}$), and the upper limit at 90% C.L. ($N^{\rm UL}$) on the signal yield for each $\Omega(2012)$ decay mode.

Mode	ε (%)	σ	$N^{\rm fit}$	$N^{\rm UL}$
$\Omega(2012)^- \to \Xi(1530)^0(\to \Xi^-\pi^+)K^-$	8.71 ± 0.06	1.8	22.5 ± 12.9	41.0
$\Omega(2012)^- \to \Xi(1530)^-(\to \Xi^-\pi^0)K^0_S$	1.26 ± 0.01	…	-3.5 ± 11.6	16.6
$\Omega(2012)^- \to \Xi(1530)^-(\to \Xi^0\pi^-)K^0_S$	2.06 ± 0.02	…	-1.0 ± 3.6	7.2
$\Omega(2012)^- \to \Xi(1530)^0(\to \Xi^0\pi^0)K^-$	0.75 ± 0.01	…	-12.0 ± 9.8	13.2

TABLE III. The values of the $\mathcal{R}^{\Xi^-\pi^+K^-}_{\Xi^-\bar{K}^0}$, $\mathcal{R}^{\Xi^-\pi^0\bar{K}^0}_{\Xi^-\bar{K}^0}$, $\mathcal{R}^{\Xi^0\pi^-\bar{K}^0}_{\Xi^0K^-}$, $\mathcal{R}^{\Xi^0\pi^0K^-}_{\Xi^0K^-}$, $\mathcal{R}^{\Xi^-\pi^+K^-}_{\Xi^0K^-}$, and $\mathcal{R}^{\Xi^0\pi^-\bar{K}^0}_{\Xi^-\bar{K}^0}$.

The ratio	The value
$\mathcal{R}^{\Xi^-\pi^+K^-}_{\Xi^-\bar{K}^0}$	$(5.0 \pm 2.9)\%$
$\mathcal{R}^{\Xi^-\pi^0\bar{K}^0}_{\Xi^-\bar{K}^0}$	$(-15.8 \pm 52.3)\%$
$\mathcal{R}^{\Xi^0\pi^-\bar{K}^0}_{\Xi^0K^-}$	$(-2.3 \pm 8.4)\%$
$\mathcal{R}^{\Xi^0\pi^0K^-}_{\Xi^0K^-}$	$(-26.8 \pm 21.9)\%$
$\mathcal{R}^{\Xi^-\pi^+K^-}_{\Xi^0K^-}$	$(4.2 \pm 2.5)\%$
$\mathcal{R}^{\Xi^0\pi^-\bar{K}^0}_{\Xi^-\bar{K}^0}$	$(-2.8 \pm 10.0)\%$

$$\mathcal{R}^{\Xi^0\pi^0K^-}_{\Xi^0K^-} = \frac{\mathcal{B}(\Omega(2012) \to \Xi(1530)^0(\to \Xi^0\pi^0)K^-)}{\mathcal{B}(\Omega(2012) \to \Xi^0K^-)} = \frac{N_4^{\rm fit} \times \varepsilon_6}{N_6^{\rm fit} \times \varepsilon_4 \times \mathcal{B}(\pi^0 \to \gamma\gamma)}, \quad (4)$$

$$\mathcal{R}^{\Xi^-\pi^+K^-}_{\Xi^0K^-} = \frac{\mathcal{B}(\Omega(2012) \to \Xi(1530)^0(\to \Xi^-\pi^+)K^-)}{\mathcal{B}(\Omega(2012) \to \Xi^0K^-)} = \frac{N_1^{\rm fit} \times \varepsilon_6 \times \mathcal{B}(\Xi^0 \to \Lambda\pi^0) \times \mathcal{B}(\pi^0 \to \gamma\gamma)}{N_6^{\rm fit} \times \varepsilon_1 \times \mathcal{B}(\Xi^- \to \Lambda\pi^-)}, \quad (5)$$

$$\mathcal{R}^{\Xi^0\pi^-\bar{K}^0}_{\Xi^-\bar{K}^0} = \frac{\mathcal{B}(\Omega(2012) \to \Xi(1530)^-(\to \Xi^0\pi^-)\bar{K}^0)}{\mathcal{B}(\Omega(2012) \to \Xi^-\bar{K}^0)} = \frac{N_3^{\rm fit} \times \varepsilon_5 \times \mathcal{B}(\Xi^- \to \Lambda\pi^-)}{N_5^{\rm fit} \times \varepsilon_3 \times \mathcal{B}(\Xi^0 \to \Lambda\pi^0) \times \mathcal{B}(\pi^0 \to \gamma\gamma)}, \quad (6)$$

where the errors are statistical only; $N_1^{\rm fit}$, $N_2^{\rm fit}$, $N_3^{\rm fit}$, $N_4^{\rm fit}$, $N_5^{\rm fit}$, and $N_6^{\rm fit}$ are the fitted signal yields in the modes $\Omega(2012)^- \to \Xi(1530)^0(\to \Xi^-\pi^+)K^-$, $\Xi(1530)^-(\to \Xi^-\pi^0)\bar{K}^0$, $\Xi(1530)^-(\to \Xi^0\pi^-)\bar{K}^0$, $\Xi(1530)^0(\to \Xi^0\pi^0)K^-$, $\Xi^-K^0_S$, and Ξ^0K^-, respectively; ε_1, ε_2, ε_3, ε_4, ε_5, and ε_6 are the corresponding efficiencies for each mode. The values of $N_1^{\rm fit}$, $N_2^{\rm fit}$, $N_3^{\rm fit}$, $N_4^{\rm fit}$, ε_1, ε_2, ε_3, and ε_4 are listed in Table II. The values of $N_5^{\rm fit}$, $N_6^{\rm fit}$, ε_5, and ε_6 are 279 ± 71, 242 ± 48, $(15.7 \pm 0.2)\%$, and $(4.0 \pm 0.1)\%$. In our calculations, we use the standard value of $\mathcal{B}(\bar{K}^0 \to K^0_S) = 0.5$. Finally, the values of the $\mathcal{R}^{\Xi^-\pi^+K^-}_{\Xi^-\bar{K}^0}$, $\mathcal{R}^{\Xi^-\pi^0\bar{K}^0}_{\Xi^-\bar{K}^0}$, $\mathcal{R}^{\Xi^0\pi^-\bar{K}^0}_{\Xi^0K^-}$, $\mathcal{R}^{\Xi^0\pi^0K^-}_{\Xi^0K^-}$, $\mathcal{R}^{\Xi^-\pi^+K^-}_{\Xi^0K^-}$, and $\mathcal{R}^{\Xi^0\pi^-\bar{K}^0}_{\Xi^-\bar{K}^0}$ are obtained; they are listed in Table III.

F. Simultaneous fit results

Considering that the branching fractions of $\Omega(2012)^- \to \Xi^-\bar{K}^0$ and $\Omega(2012)^- \to \Xi^0K^-$ and the ratios of branching fractions of the three-body decay modes of $\Omega(2012)$ are known, the ratio of expected signal yields between each $\Omega(2012)$ three-body decay mode can be calculated. With such constraints, we perform a simultaneous fit to obtain the upper limit on $\mathcal{R}^{\Xi\pi K}_{\Xi K} = \mathcal{B}(\Omega(2012) \to \Xi(1530)(\to \Xi\pi)K)/\mathcal{B}(\Omega(2012) \to \Xi K)$.

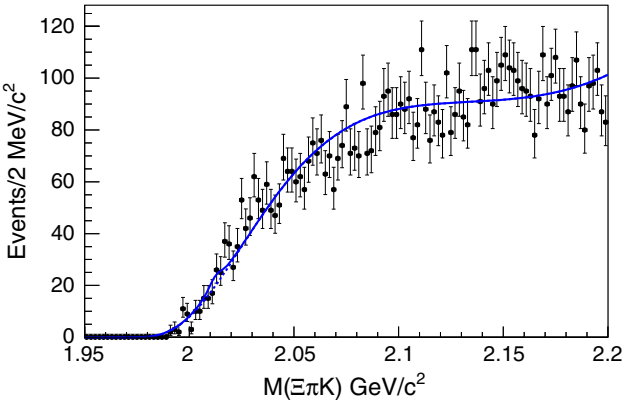

FIG. 5. The final simultaneous fit result to all three-body $\Omega(2012)$ decay modes from the combined $\Upsilon(1S, 2S, 3S)$ data samples. The solid curve is the best fit, and the dashed line represents the backgrounds.

Taking $\mathcal{B}(\Omega(2012)^- \to \Xi^-\bar{K}^0) : \mathcal{B}(\Omega(2012)^- \to \Xi^0K^-) = 1.0 : 1.2$ [1] and $\mathcal{B}(\Omega(2012)^- \to \Xi(1530)^0(\to \Xi^-\pi^+)K^-) : \mathcal{B}(\Omega(2012)^- \to \Xi(1530)^-(\to \Xi^-\pi^0)\bar{K}^0) : \mathcal{B}(\Omega(2012)^- \to \Xi(1530)^-(\to \Xi^0\pi^-)\bar{K}^0) : \mathcal{B}(\Omega(2012)^- \to \Xi(1530)^0(\to \Xi^0\pi^0)K^-) = 2 : 1 : 2 : 1$ according to isospin symmetry, we derive that $\mathcal{R}^{\Xi^-\pi^+K^-}_{\Xi^-\bar{K}^0} : \mathcal{R}^{\Xi^-\pi^0\bar{K}^0}_{\Xi^-\bar{K}^0} : \mathcal{R}^{\Xi^0\pi^-\bar{K}^0}_{\Xi^0K^-} : \mathcal{R}^{\Xi^0\pi^0K^-}_{\Xi^0K^-} = 1 : \frac{1}{2} : \frac{1}{1.2} : \frac{1}{2.4}$. Thus, according to Eqs. (1)–(4), we have:

$$N_1^{\rm fit} : N_2^{\rm fit} : N_3^{\rm fit} : N_4^{\rm fit} = 87.2\% : 2.2\% : 7.0\% : 3.6\%. \quad (7)$$

An unbinned extended maximum-likelihood simultaneous fit to all three-body decay modes is now performed. In the simultaneous fit, the ratios of the expected observed $\Omega(2012)$ signals between each decay channel are fixed according to Eq. (7). The functions used to describe the signal and background shapes are parametrized as before. The fit result is shown in Fig. 5 from the combined $\Upsilon(1S, 2S, 3S)$ data samples, corresponding to a total fit yield of 22.4 ± 14.0. The statistical significance of the $\Omega(2012)$ signal is 1.6σ. Finally, we determine

$$\mathcal{R}^{\Xi\pi K}_{\Xi K} = \frac{\mathcal{B}(\Omega(2012) \to \Xi(1530)(\to \Xi\pi)K)}{\mathcal{B}(\Omega(2012) \to \Xi K)} = (6.0 \pm 3.7(\text{stat}) \pm 1.3(\text{syst}))\%, \quad (8)$$

where $\mathcal{B}(\Omega(2012) \to \Xi(1530)(\to \Xi\pi)K) = \mathcal{B}(\Omega(2012)^- \to \Xi(1530)^0(\to \Xi^-\pi^+)K^-) + \mathcal{B}(\Omega(2012)^- \to \Xi(1530)^-(\to \Xi^-\pi^0)\bar{K}^0) + \mathcal{B}(\Omega(2012)^- \to \Xi(1530)^-(\to \Xi^0\pi^-)\bar{K}^0) + \mathcal{B}(\Omega(2012)^- \to \Xi(1530)^0(\to \Xi^0\pi^0)K^-)$ and $\mathcal{B}(\Omega(2012) \to \Xi K) = \mathcal{B}(\Omega(2012)^- \to \Xi^-\bar{K}^0) + \mathcal{B}(\Omega(2012)^- \to \Xi^0K^-)$. In the calculations, each branching fraction is determined individually. Systematic uncertainties are detailed below.

G. Systematic uncertainties

We now discuss the systematic uncertainties inherent in our measurements of the ratios $\mathcal{R}^{\Xi^-\pi^+K^-}_{\Xi^-\bar{K}^0}$, $\mathcal{R}^{\Xi^-\pi^0\bar{K}^0}_{\Xi^-\bar{K}^0}$, $\mathcal{R}^{\Xi^0\pi^-\bar{K}^0}_{\Xi^0K^-}$, $\mathcal{R}^{\Xi^0\pi^0K^-}_{\Xi^0K^-}$, $\mathcal{R}^{\Xi^-\pi^+K^-}_{\Xi^0K^-}$, $\mathcal{R}^{\Xi^0\pi^-\bar{K}^0}_{\Xi^-\bar{K}^0}$, and $\mathcal{R}^{\Xi\pi K}_{\Xi K}$. These include detection efficiency (tracking efficiency, kaon and pion particle ID, Λ, K^0_S, and π^0 reconstruction), the statistical error in the MC efficiency, the branching fractions of possible intermediate states, the $\Omega(2012)$ resonance parameters, any possible bias in reconstructed mass (as evaluated from the difference between the reconstructed Ξ^0 mass and the world average value), as well as the overall fit uncertainty.

Based on a study of $D^{*+} \to D^0(\to K^0_S\pi^+\pi^-)\pi^+$, the uncertainty in tracking efficiency is taken to be 0.35% per track. The uncertainties in particle identification are studied via a low-background sample of D^* decay for charged kaons and pions. The studies show uncertainties of 1.3% for each charged kaon and 1.1% for each charged pion. The uncertainty in Λ selection is 3% [21]. Differences in K^0_S selection efficiency determined from data and MC simulation give a relation of $1 - \varepsilon_{\rm data}/\varepsilon_{\rm MC} = (1.4 \pm 0.3)\%$ [22]; 1.7% is taken as a conservative systematic uncertainty. For π^0 reconstruction, the efficiency correction and systematic uncertainty are estimated from a sample of $\tau^- \to \pi^-\pi^0\nu$. We find a 2.25% systematic uncertainty on π^0 reconstruction efficiency. In the measurements of $\mathcal{R}^{\Xi^-\pi^+K^-}_{\Xi^-\bar{K}^0}$, $\mathcal{R}^{\Xi^-\pi^0\bar{K}^0}_{\Xi^-\bar{K}^0}$, $\mathcal{R}^{\Xi^0\pi^-\bar{K}^0}_{\Xi^0K^-}$, $\mathcal{R}^{\Xi^-\pi^+K^-}_{\Xi^0K^-}$, $\mathcal{R}^{\Xi^0\pi^-\bar{K}^0}_{\Xi^-\bar{K}^0}$, and $\mathcal{R}^{\Xi^0\pi^0K^-}_{\Xi^0K^-}$, the common sources of systematic uncertainties such as Ξ selection cancel; the individual errors are summed in quadrature to obtain the total detection efficiency uncertainty. For the measurement of $\mathcal{R}^{\Xi\pi K}_{\Xi K}$, to determine the total detection efficiency, the systematic errors for each final state and the errors from tracking, particle identification, Λ, K^0_S, and π^0 reconstruction are first summed in quadrature to obtain σ_i. Then, the total systematic uncertainty for detection efficiency ($\sigma_{\rm DE}$) is determined using standard error propagation as follows:

$$\sigma_{\rm DE} = \sqrt{\frac{\Sigma_i(\mathcal{W}_i \times \sigma_i)^2}{(\Sigma_i \mathcal{W}_i)^2} + \frac{\Sigma_j(\mathcal{W}_j \times \sigma_j)^2}{\Sigma_j(\mathcal{W}_j)^2}} = 7.3\% \qquad (9)$$

Here, $\mathcal{W}_i$ is the weight factor of the branching fraction in the ith ($i = 0, 1, 2, 3$) mode of the $\Omega(2012) \to \Xi\pi K$ decay; $\mathcal{W}_j$ ($j = 0, 1$) is the relative weight for the jth mode of $\Omega(2012) \to \Xi K$ decay.

The statistical uncertainty in the determination of the efficiency from MC simulations is less than 1.0%. In the calculation of $\mathcal{R}^{\Xi\pi K}_{\Xi K}$, only the branching fractions of intermediate states $\mathcal{B}(K^0_S \to \pi^+\pi^-)$ and $\mathcal{B}(\pi^0 \to \gamma\gamma)$ are included; the corresponding uncertainties are 0.072% and 0.035% [2], respectively, which are sufficiently small to be neglected. The uncertainty in the $\Omega(2012)$ resonance parameters is estimated by toggling the values of resonance mass and width by $\pm 1\sigma$ and refitting. The largest differences compared to the nominal fit results are taken as the systematic uncertainties associated with the $\Omega(2012)$ resonance parameters. The uncertainty in the Ξ^0 mass is estimated by comparing the numbers of the signal yields of the $\Omega(2012)$ for the case where the mass of the reconstructed Ξ^0 is fixed at the found peak value versus the case where the mass is fixed to the nominal mass [2]. According to the $\Xi(1530)K$ invariant mass distributions in inclusive MC samples, we find that the threshold mass value falls within the $[1.96, 1.98]$ GeV/c^2 interval. The systematic error in the background parametrization is estimated by comparing the yields when the threshold mass is changed by ± 10 MeV/c^2 relative to the nominal fit (for which the threshold is fixed at 1.97 GeV/c^2). By extending the fitted region of the $M(\Xi\pi K)$, e.g., 2.2 to 2.3 GeV/c^2, the upper limits at 90% C.L. on the $\Omega(2012)$ signal yields are not changed. Such systematic uncertainty due to the fit region can be neglected.

All the uncertainties are summarized in Table IV, and, assuming all errors are independent, summed in quadrature to give the total systematic uncertainty.

H. 90% C.L. upper limits

In the absence of any significant observed signals, upper limits at 90% C.L. on the $\mathcal{R}^{\Xi^-\pi^+K^-}_{\Xi^-\bar{K}^0}$, $\mathcal{R}^{\Xi^-\pi^0\bar{K}^0}_{\Xi^-\bar{K}^0}$, $\mathcal{R}^{\Xi^0\pi^-\bar{K}^0}_{\Xi^0K^-}$, $\mathcal{R}^{\Xi^0\pi^0K^-}_{\Xi^0K^-}$, $\mathcal{R}^{\Xi^-\pi^+K^-}_{\Xi^0K^-}$, $\mathcal{R}^{\Xi^0\pi^-\bar{K}^0}_{\Xi^-\bar{K}^0}$, and $\mathcal{R}^{\Xi\pi K}_{\Xi K}$ modes are determined by solving the equation

TABLE IV. Relative systematic errors (%) on the measurements of $\mathcal{R}^{\Xi^-\pi^+K^-}_{\Xi^-\bar{K}^0}$, $\mathcal{R}^{\Xi^-\pi^0\bar{K}^0}_{\Xi^-\bar{K}^0}$, $\mathcal{R}^{\Xi^0\pi^-\bar{K}^0}_{\Xi^0K^-}$, $\mathcal{R}^{\Xi^0\pi^0K^-}_{\Xi^0K^-}$, $\mathcal{R}^{\Xi^-\pi^+K^-}_{\Xi^0K^-}$, $\mathcal{R}^{\Xi^0\pi^-\bar{K}^0}_{\Xi^-\bar{K}^0}$, and $\mathcal{R}^{\Xi\pi K}_{\Xi K}$.

Source	$\mathcal{R}^{\Xi^-\pi^+K^-}_{\Xi^-\bar{K}^0}$	$\mathcal{R}^{\Xi^-\pi^0\bar{K}^0}_{\Xi^-\bar{K}^0}$	$\mathcal{R}^{\Xi^0\pi^-\bar{K}^0}_{\Xi^0K^-}$	$\mathcal{R}^{\Xi^0\pi^0K^-}_{\Xi^0K^-}$	$\mathcal{R}^{\Xi^-\pi^+K^-}_{\Xi^0K^-}$	$\mathcal{R}^{\Xi^0\pi^-\bar{K}^0}_{\Xi^-\bar{K}^0}$	$\mathcal{R}^{\Xi\pi K}_{\Xi K}$
Detection efficiency	2.5	3.4	2.6	3.0	3.3	3.3	7.3
MC statistics	1.0	1.0	1.0	1.0	1.0	1.0	1.0
$\Omega(2012)$ resonance parameters	10.7	33.5	41.3	27.8	10.7	41.3	6.1
Ξ^0 mass	…	…	17.4	3.3	…	17.4	4.5
Background parameter	7.9	23.4	30.0	17.2	7.9	30.0	18.1
Sum in quadrature	13.6	41.0	54.0	33.0	13.7	54.1	21.0

$$\int_0^{t^{\rm UL}} \mathcal{F}_{\rm likelihood}(t)dt \Big/ \int_0^{+\infty} \mathcal{F}_{\rm likelihood}(t)dt = 90\%, \quad (10)$$

where t is the assumed ratio of branching fractions, and $\mathcal{F}_{\rm likelihood}(t)$ is the corresponding maximized likelihood of the data. To take into account systematic uncertainties, the likelihood is convolved with a Gaussian function whose width equals the corresponding total systematic uncertainty. Finally, we obtain

$$\mathcal{R}^{\Xi^-\pi^+K^-}_{\Xi^-\bar{K}^0} = \frac{\mathcal{B}(\Omega(2012)\to\Xi(1530)^0(\to\Xi^-\pi^+)K^-)}{\mathcal{B}(\Omega(2012)\to\Xi^-\bar{K}^0)} < 9.3\%, \quad (11)$$

$$\mathcal{R}^{\Xi^-\pi^0\bar{K}^0}_{\Xi^-\bar{K}^0} = \frac{\mathcal{B}(\Omega(2012)\to\Xi(1530)^-(\to\Xi^-\pi^0)\bar{K}^0)}{\mathcal{B}(\Omega(2012)\to\Xi^-\bar{K}^0)} < 81.1\%, \quad (12)$$

$$\mathcal{R}^{\Xi^0\pi^-\bar{K}^0}_{\Xi^0K^-} = \frac{\mathcal{B}(\Omega(2012)\to\Xi(1530)^-(\to\Xi^0\pi^-)\bar{K}^0)}{\mathcal{B}(\Omega(2012)\to\Xi^0K^-)} < 21.3\%, \quad (13)$$

$$\mathcal{R}^{\Xi^0\pi^0K^-}_{\Xi^0K^-} = \frac{\mathcal{B}(\Omega(2012)\to\Xi(1530)^0(\to\Xi^0\pi^0)K^-)}{\mathcal{B}(\Omega(2012)\to\Xi^0K^-)} < 30.4\%, \quad (14)$$

$$\mathcal{R}^{\Xi^-\pi^+K^-}_{\Xi^0K^-} = \frac{\mathcal{B}(\Omega(2012)\to\Xi(1530)^0(\to\Xi^-\pi^+)K^-)}{\mathcal{B}(\Omega(2012)\to\Xi^0K^-)} < 7.8\%, \quad (15)$$

$$\mathcal{R}^{\Xi^0\pi^-\bar{K}^0}_{\Xi^-\bar{K}^0} = \frac{\mathcal{B}(\Omega(2012)\to\Xi(1530)^-(\to\Xi^0\pi^-)\bar{K}^0)}{\mathcal{B}(\Omega(2012)\to\Xi^-\bar{K}^0)} < 25.6\%, \quad (16)$$

and

$$\mathcal{R}^{\Xi\pi K}_{\Xi K} = \frac{\mathcal{B}(\Omega(2012)\to\Xi(1530)(\to\Xi\pi)K)}{\mathcal{B}(\Omega(2012)\to\Xi K)} < 11.9\% \quad (17)$$

at 90% C.L.

IV. RESULTS AND DISCUSSION

In summary, using the data samples of 5.7 fb^{-1} $\Upsilon(1S)$, 24.9 fb^{-1} $\Upsilon(2S)$, and 2.9 fb^{-1} $\Upsilon(3S)$ collected by the Belle detector, we have searched for the three-body $K\pi\Xi$ decay of $\Omega(2012)$ for the first time. No significant signals are observed, and we determine upper limits at 90% C.L. on the ratios of $\mathcal{R}^{\Xi^-\pi^+K^-}_{\Xi^-\bar{K}^0}$, $\mathcal{R}^{\Xi^-\pi^0\bar{K}^0}_{\Xi^-\bar{K}^0}$, $\mathcal{R}^{\Xi^0\pi^-\bar{K}^0}_{\Xi^0K^-}$, $\mathcal{R}^{\Xi^0\pi^0K^-}_{\Xi^0K^-}$, $\mathcal{R}^{\Xi^-\pi^+K^-}_{\Xi^0K^-}$, $\mathcal{R}^{\Xi^0\pi^-\bar{K}^0}_{\Xi^-\bar{K}^0}$, and $\mathcal{R}^{\Xi\pi K}_{\Xi K}$ to be 9.3%, 81.1%, 21.3%, 30.4%, 7.8%, 25.6%, and 11.9%, respectively. Our result strongly disfavors the molecular interpretation proposed by Ref. [7], and is in tension with the predictions of Refs. [8–11], also based on molecular interpretations.

ACKNOWLEDGMENTS

S. J. acknowledges the support from the China Scholarship Council under No. 201706020133 and the Academic Excellence Foundation of BUAA for PhD students. We thank the KEKB group for the excellent operation of the accelerator; the KEK cryogenics group for the efficient operation of the solenoid; and the KEK computer group, and the Pacific Northwest National Laboratory (PNNL) Environmental Molecular Sciences Laboratory (EMSL) computing group for strong computing support; and the National Institute of Informatics, and Science Information NETwork 5 (SINET5) for valuable network support. We acknowledge support from the Ministry of Education, Culture, Sports, Science, and Technology (MEXT) of Japan, the Japan Society for the Promotion of Science (JSPS), and the Tau-Lepton Physics Research Center of Nagoya University; the Australian Research Council including Grants No. DP180102629, No. DP170102389, No. DP170102204, No. DP150103061, No. FT130100303; Austrian Science Fund (FWF); the National Natural Science Foundation of China under Contracts No. 11435013, No. 11475187, No. 11521505, No. 11575017, No. 11675166, No. 11705209, No. 11761141009; Key Research Program of Frontier Sciences, Chinese Academy of Sciences (CAS), Grant No. QYZDJ-SSW-SLH011; the CAS Center for Excellence in Particle Physics (CCEPP); the Shanghai Pujiang Program under Grant No. 18PJ1401000; the Ministry of Education, Youth and Sports of the Czech Republic under Contract No. LTT17020; the Carl Zeiss Foundation, the Deutsche Forschungsgemeinschaft, the Excellence Cluster Universe, and the VolkswagenStiftung; the Department of Science and Technology of India; the Istituto Nazionale di Fisica Nucleare of Italy; National Research Foundation (NRF) of Korea Grants No. 2015H1A2A1033649, No. 2016R1D1A1B01010135, No. 2016K1A3A7A09005603, No. 2016R1D1A1B02012900, No. 2018R1A2B3003643, No. 2018R1A6A1A06024970, No. 2018R1D1A1B07047294; Radiation Science Research Institute, Foreign Large-size Research Facility Application Supporting project, the Global Science Experimental Data Hub Center of the Korea Institute of Science and Technology Information and KREONET/GLORIAD; the Polish Ministry of Science and Higher Education and the National Science Center; the Grant of the Russian Federation Government, Agreement No. 14.W03.31.0026; the Slovenian Research Agency; Ikerbasque, Basque Foundation for Science, Spain; the Swiss National Science Foundation; the Ministry of Education and the Ministry of Science and Technology of Taiwan; and the United States Department of Energy and the National Science Foundation.

[1] J. Yelton *et al.* (Belle Collaboration), Phys. Rev. Lett. **121**, 052003 (2018).
[2] M. Tanabashi *et al.* (Particle Data Group), Phys. Rev. D **98**, 030001 (2018).
[3] L. Y. Xiao and X. H. Zhong, Phys. Rev. D **98**, 034004 (2018).
[4] T. M. Aliev, K. Azizi, Y. Sarac, and H. Sundu, Eur. Phys. J. C **78**, 894 (2018).
[5] T. M. Aliev, K. Azizi, Y. Sarac, and H. Sundu, Phys. Rev. D **98**, 014031 (2018).
[6] Z. Y. Wang, L. C. Gui, Q. F. Lu, L. Y. Xiao, and X. H. Zhong, Phys. Rev. D **98**, 114023 (2018).
[7] Y. H. Lin and B. S. Zou, Phys. Rev. D **98**, 056013 (2018).
[8] M. P. Valderrama, Phys. Rev. D **98**, 054009 (2018).
[9] Y. Huang, M. Z. Liu, J. X. Lu, J. J. Xie, and L. S. Geng, Phys. Rev. D **98**, 076012 (2018).
[10] R. Pavao and E. Oset, Eur. Phys. J. C **78**, 857 (2018).
[11] M. V. Polyakov, H. D. Son, B. D. Sun, and A. Tandogan, Phys. Lett. B **792**, 315 (2019).
[12] S. Kurokawa and E. Kikutani, Nucl. Instrum. Methods Phys. Res., Sect. A **499**, 1 (2003), and other papers included in this volume.
[13] T. Abe *et al.*, Prog. Theor. Exp. Phys. **2013**, 03A001 (2013) and references therein.
[14] A. Abashian *et al.* (Belle Collaboration), Nucl. Instrum. Methods Phys. Res., Sect. A **479**, 117 (2002).
[15] J. Brodzicka *et al.*, Prog. Theor. Exp. Phys. **2012**, 04D001 (2012).
[16] D. J. Lange, Nucl. Instrum. Methods Phys. Res., Sect. A **462**, 152 (2001).
[17] T. Sjöstrand, S. Mrenna, and P. Skands, J. High Energy Phys. 05 (2006) 026.
[18] M. Feindt and U. Kerzel, Nucl. Instrum. Methods Phys. Res., Sect. A **559**, 190 (2006).
[19] H. Nakano, Chapter 4, Ph.D. Thesis, Tohoku University, 2014.
[20] In common high energy physics usage, this Bayesian interval has been reported as "confidence interval," which is a frequentist-statistics term.
[21] Y. Kato *et al.* (Belle Collaboration), Phys. Rev. D **94**, 032002 (2016).
[22] N. Dash *et al.* (Belle Collaboration), Phys. Rev. Lett. **119**, 171801 (2017).